Experimental investigation and finite element modelling of microstructural composite material

Henri-Alexandre Cayzac, Lucien Laiarinandrasana, Sébastien Joannès

EXPERIMENTAL INVESTIGATION AND FINITE ELEMENT MODELLING OF MICROSTRUCTURAL COMPOSITE MATERIAL

H.A. Cayzac[1*], L. Laiarinandrasana[1], S. Joannes[1]

[1]*Mines Paristech, Centre des Matériaux, CNRS UMR 7633,BP 87, 91003 Evry Cedex, France*
**henri.cayzac@mines-paristech.fr*

Keywords: microstructure, variability, tomography-X, damage

Abstract
Experimental investigations on PA6GF composite material through SEM images showed high microstructural variability. Local fibre volume fractions were quantified. The use of X-ray tomography techniques allowed examinations of matrix damage mechanisms by void growth. A constitutive model for bulk PA6 polymer was set up in order to simulate PA6 behavior submitted to complex triaxial loadings. Unit cell computations were then carried out to better understand the influence of hydrostatic pressure on composite materials.

1 Introduction

The use of composite materials for gas transportation has recently known a growing interest. New designed pipes made of an inner polymer core which provides hermetical sealing, wrapped with a composite material enhancing mechanical properties are emerging. The inner core is composed of thermoplastic semi-crystalline polymer while the outer composite shell is made of thermoplastic polymer reinforced with unidirectional continuous fibers. The present contribution is devoted to highlight microstructural variability and to take it into account in finite element models.

2 Experimental investigations

2.1 Material

The material under study is a Polyamide 6 (PA6) matrix reinforced with unidirectional continuous Glass Fibres (GF) referred to as PA6GF. This material is produced through a pultrusion process that allows high fibre volume fraction. Global fibre volume fraction was determined on pyrolysed sample. Such experiment consisting in burning the polymeric particules at high temperatures (here temperature was set up at 650 °C) and keeping fibres intact. The fibre volume fraction close to 70% was estimated.

2.2 Microstructural variability

Transverse cross-sections as well as longitudinal sections of undamaged PA6GF composite were observed thanks to Scanning Electron Microscopy (SEM) techniques. Composite samples are embedded in a polymeric matrix and carefully polished. Fig.1 illustrates a SEM microscopic image of a composite transverse cross-section. Undamaged material shows high microstructural variability. Indeed different fibre diameter can be clearly observed on Fig.1. Diameter distribution was quantified on several SEM microstructure images thanks to the use of digital image processing (Matlab software). 8000 fibres were randomly selected from

microstructure images in order to establish the average diameter size: 15.1±0.05µm. Fibre diameter distribution has not yet been taken into account in our numerical models.

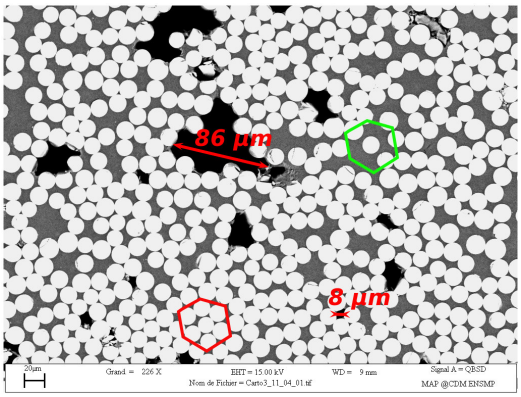

Figure 1. PA6GF transverse cross-section (SEM).

Voids can also be observed in Fig.1, they take place in the polymer matrix between fibres. Voids have various diameter sizes ranging from few µm to 100µm. Longitudinal sections showed that voids have "rice" grain size i.e. the longitudinal size is much longer than the diametrical one. Such voids are due to the pultrusion process when air bubbles get stuck between fibres.

The local fibre area fraction distribution defined as the ratio of fibres area over an observed Surface Of Interest (SOI) was quantified. The local SOI is chosen as a square area of 625 µm². The average fibre area is around 170 µm² therefore a maximum of 3.7 fibres can fit into a single SOI. A total of 39 SEM images of microstructure were used and each of them was divided into sereval SOI's. Therefore a total of 10920 SOI's were set up. On each SOI the local fibre area fraction is calculated. Results are shown on Fig.2. It is assumed that the local fibre area fraction correspond to the local volume fraction. The average local volume fraction was estimated at 65.6 ± 6.8%. A large distribution in the local fibre volume fraction was highlighted. Indeed local volume fractions from 40% to 80% were recorded while square packing volume fraction is 78.5%. Half of the overall local fibre volume fraction calculated is upper than 65%.

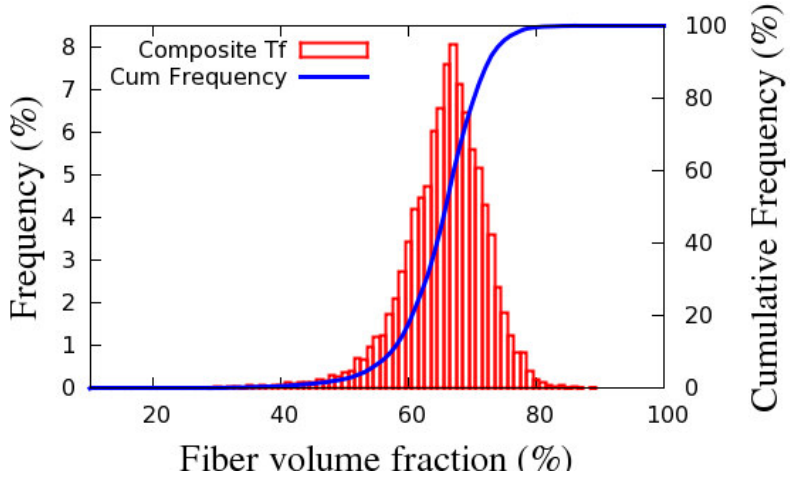

Figure 2. Fibre volume fraction distribution.

Polymer materials are highly sensitive to hydrostatic pressure; such local volume fraction distribution is expected to have an impact on mechanical behavior and damage mechanisms.

2.3 X-ray tomography

X-ray tomography is a non destructive 3D observation technique that has recently known a growing interest. This technique consisting in scanning small volumes provides high resolution 3D images allowing in situ observation and damage characterization [1].

Laminography experiments [2] were set up on bands of 1.5 mm thick. Specimens were notched either in the longitudinal direction or in the transverse one. Initiation and propagation of cracks are due to a device allowing a displacement between the two edges of the notch [2]. The experiment consists in scanning the initial microstructure, applying a displacement between the notch edges in order to propagate cracks, scanning the microstructure and so on up to the total failure of the specimen. Therefore in situ damage can be characterized in transverse and longitudinal directions.

Figure 3. X-ray tomography images. (a) Initial microstructure with voids; (b) Microstructure after deformation: void growth.

Initial scans corresponding to undamaged material were assessed with the help of SEM inspections. Indeed voids exhibit "rice grain" shape and dimension along fibres can be much higher than diametrical dimensions. Whatever the implantation of the notch, parallel or perpendicular to the fibre direction, the main crack always propagates through the matrix in the fibre direction due to the high isotropy of the material. Fig.3(a) represents initial voids in the composite material. This volume is located far from the notch root. These voids are probably due to a lack of matrix polymer between fibres. Fig.3(b) shows the same volume after deformation of the sample. Voids have clearly grown and are likely to coalesce to lead to a cylindrical crack. The space between voids gets smaller, thin polymer walls are separating voids. It is assumed that damage mechanism in the matrix under such solicitation is based on void growth.

2.4 Hydrostatic pressure on bulk polymer

Recent studies on bulk polymer materials have shown that stress triaxiality ratio (hydrostatic pressure) have a strong influence on damage mechanisms [3] [4] [5]. Whitening of polymers was related to void growth leading to a significant volume change in the polymeric material [6]. It was reported that the hydrostatic pressure played a major role on the damage growth mechanisms. Different tensile or compressive tests on notched axi-symmetrical specimens were performed. Such specimens are devoted to study the effect of hydrostatic pressure. SEM

analysis [3] assessed with recent X-tomography analysis on interrupted tensile notched specimens tests have showed the microstructural evolution of polymer PA6 or PA11 in deformation. In addition the damage distribution (voids nucleation and growth) were spatially and chronologically quantified.

3 Microstructural variability in FEM models

In this section, experimental results were used in order to implement in finite element models constitutive equations for the polymeric matrix and analyze the effect of microstructural variability.

3.1 Bulk PA6 constitutive model

A viscoplastic multi-mechanism based model [7] [8] were implemented in a in house Finite Element Model (FEM) code [9] in order to simulate the thermoplastic semi-crystalline polymer mechanical response to tensile tests of different notched specimens. The modified Gurson-Tvergaard-Needleman model [10] [11] [3] [5] incorporating the porosity as a damage variable was set up to simulate the damage mechanisms.

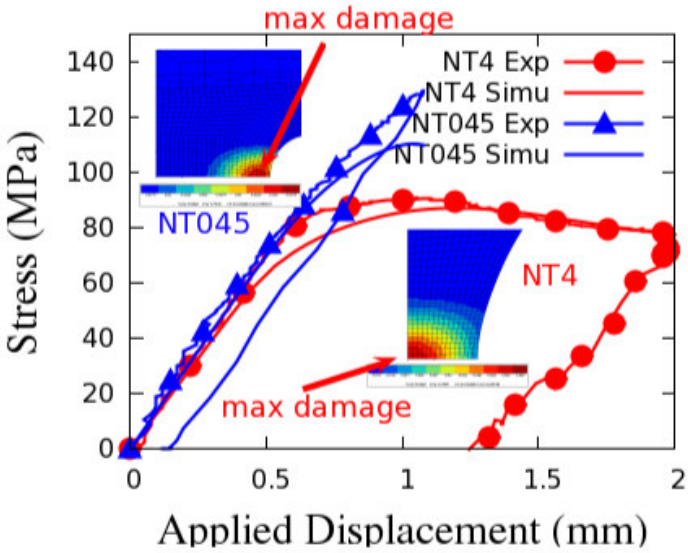

Figure 4. Net stress vs. applied displacement curves at two different notched root radii.

Identification of material coefficients was performed by utilizing the global variables obtained from experimental measures on axisymmetrical specimens containing various notch root radii. Additionally, local variables such as spatial and temporal void distributions were taken into consideration for the material coefficients optimization. Fig.4 shows experimental (lines with symbols) and simulated (lines) tensile curves of two notched specimen with different radii. The first one (NT4) have a notch radius of 4mm while the other NT045 have only 0.45mm. NT4 tensile test curve is composed of different steps. The first one, up to the peek stress is composed of the elastic deformation and the beginning of the viscoplastic one. During this step there is little volume change. The peak stress was observed to be the start of NT4 specimen re-necking. The second step corresponds to the post yielding stress softening which lead to a plateau stress. During this step, volume change occurs. Then the failure of the specimen occurs. NT045 tensile curve represents only the first stage up to the peak stress. Indeed failure of the specimens arises soon after peak stress. Fig.4 shows that there is a good

agreement between experimental and simulated results. The damage distribution can be observed on meshes of Fig.4. For NT4 the maximum damage is located in the center while for NT045 the maximum is located near the notch root. This is in agreement with the SEM observation on PA11 [3].
The present constitutive model is able to distinguish the location of maximum damage depending on the stress triaxiality ratio. It will therefore be used in order to simulate PA6 matrix behavior of PA6GF composite according to the local fibre volume fraction.

3.2 Unit cell model

3.2.1 Description of the model

A unit cell model was elaborated in order to study the influence of fibre volume fraction on hydrostatic pressure. Four different axisymmetric unit cells composed of a single fibre embedded in polymeric matrix Fig.5 (a) were selected in order to be representative of the experimental fiber volume fraction distribution (Fibre volume fraction: τ_f = 0.55, 0.6, 0.7, 0.785). Geometries of unit cells are calculated thanks to the following equation (eq.1).

$$re = \frac{ri}{\sqrt{\tau_f}} \tag{1}$$

where re is the outer matrix radius, ri the inner matrix radius (the fiber radius) and τ_f the fibre volume fraction.

The fibre was supposed to be isotropic elastic while the above mentioned damage based constitutive model was used for the polymeric matrix. The contact between the fiber and the matrix is supposed to be perfect. A displacement is imposed on the top edge of the cell, two axisymmetrical conditions are applied to the bottom and left edges. To handle the effect of hydrostatic pressure, the right edge is blocked in the radial direction. Therefore the unit cell is submitted to a pure volume variation. These drastic conditions are linked to the constraint effects. Indeed when fibre volume fraction is high enough and the composite material is under complex solicitations, polymeric matrix is constrained between fibres. An example of the contour map of the stress triaxiality ratio calculated for τ_f = 0.7 and for an applied displacement of 0.05mm is represented on Fig.5 (b).

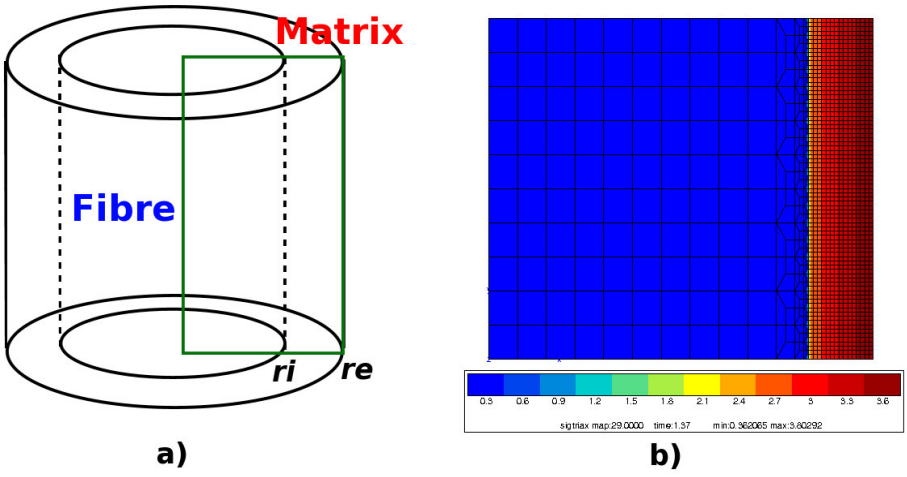

Figure 5. (a) Unit cell geometry; (b) contour map of the stress triaxiality ratio.

3.2.1 Main results

Let τ_σ be the stress triaxiality ratio, defined as:

$$\tau_\sigma = \frac{\sigma_h}{\sigma_{eq}} \tag{2}$$

where σ_h is the hydrostatic pressure defined (eq. 3) and σ_{eq} is the equivalent Mises stress.

$$\sigma_h = \frac{trace(\sigma_p)}{3} \tag{3}$$

where σ_p is the principal stress tensor.

For a given value of applied displacement, stress gradient was observed within the matrix. Principal stresses (σ_{p1} σ_{p2} σ_{p3}) and stress triaxiality ratio τ_σ in the matrix versus radial normalized coordinate is represented in Fig.6 for τ_f = 0.7 and for an applied displacement of 0.02mm. High values of the three principal stresses were observed, leading to high stress triaxiality ratio values (higher than 3) due to drastic boundary conditions. Therefore, in the following, the stress triaxiality ratio values will be systematically normalized by τ_σ = 3. It also can be observed that τ_σ is higher in the neighbouring of the right edge. As a consequence an Integration Point (IP) was selected close to this location. The IP position in the matrix is represented in Fig.6.

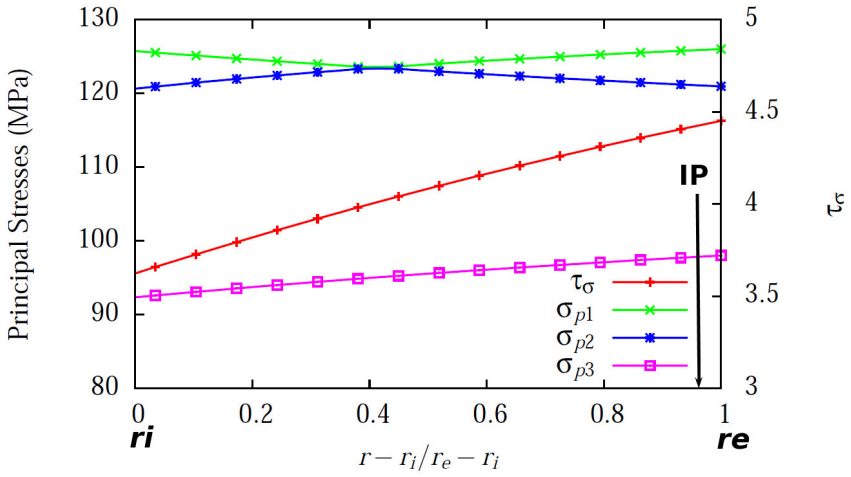

Figure 6. Principal stresses and stress triaxiality ratio inside the matrix at Mises peak stress.

At this IP, Mises stress was plotted against the applied displacement (Fig.7 (a)) according to each τ_f. Mises stress versus applied displacement curves show similar steps to NT4 stress versus displacement steps in Fig.4.

The normalized stress triaxiality ratio $\tau_\sigma/3$ against the applied displacement is plotted on Fig.7 (b). Early in the calculation, $\tau_\sigma/3$ is constant due to the matrix elastic behavior but increases when peaks stress are reached. It then decreases after the end of the stress softening stage [3]. We now select $\tau_\sigma/3$ values at Mises stress peak (symbols) to highlight the influence of τ_f versus $\tau_\sigma/3$ Fig.7 (c). This graph shows that an increase of 30% in the fiber volume fraction lead to an increase of 18% in normalized stress triaxiality ratio. The influence of the proximity of fibres will be investigated through homogenization theory.

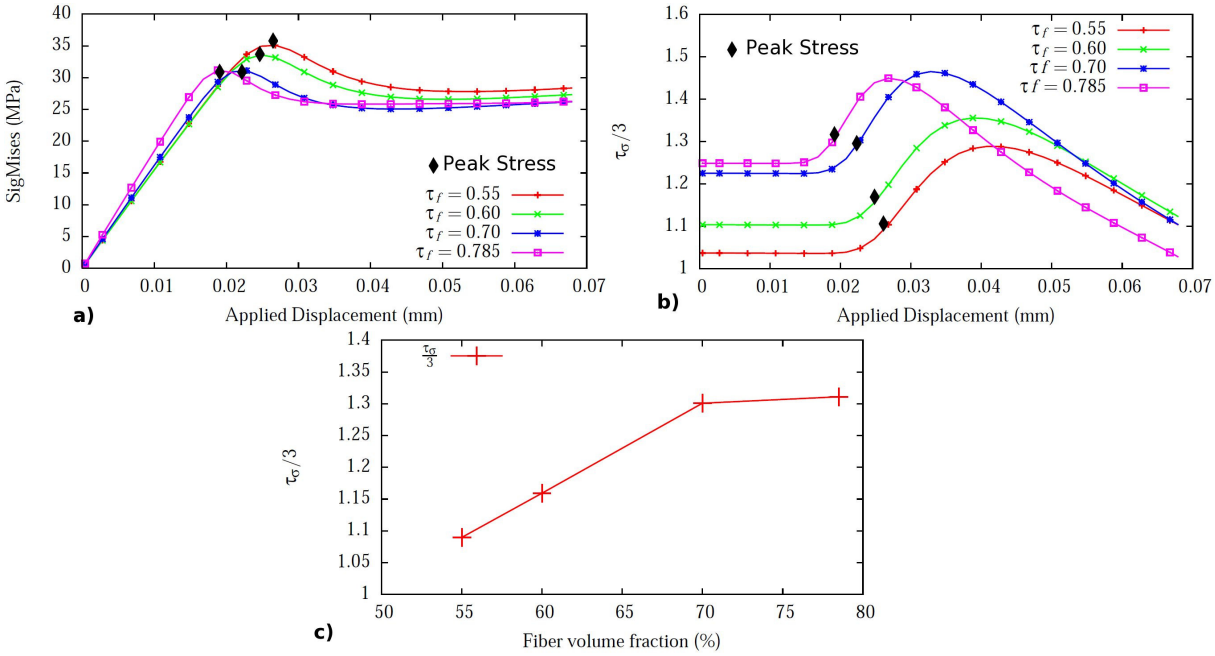

Figure 7. (a) Mises stress versus applied displacement for each fiber volume fraction; (b) hydrostatic pressure versus applied displacement; (c) hydrostatic pressure versus fiber volume fraction.

4 Conclusions

Microstructural variability of PA6GF was quantified thanks to SEM image analysis. A great interest was given to the local fibre volume fraction distribution. In situ damage evolution was characterised with X-ray tomography technique. A constitutive damage based model was investigated in order to simulate polymeric matrix behavior. Material parameters were optimized with global (stress vs. displacement curves) and local (spatial porosity distribution) variables. A unit cell model was set up in order to demonstrate that local fibre volume fraction has a strong influence on the hydrostatic pressure.

References

[1] A.J. Moffat and P. Wright and L. Helfen and T. Baumbach and G. Johnson and S.M. Spearing and I. Sinclair, *In situ synchrotron computed laminography of damage in carbon fibre-epoxy [90/0]s laminates*, Elsevier, (2009).

[2] E. Maire and T. Morgeneyer and C. Landron and J. Adrien and L. Helfen, *Bulk evaluation of ductile damage development using high resolution tomography and laminography*, Comptes Rendus Physique, (2012).

[3] G. Boisot and L. Laiarinandrasana and J. Besson and C. Fond and G. Hochstetter, *Experimental investigation and modelling of volume change induced by void growth in polyamide 11*, International Journal of Solids and Structures, (2011).

[4] E. Ghorbel, *A viscoplastic constitutive model for polymeric materials*, International Journal of Plasticity, (2008).

[5] M. Challier and J.Besson and L.Laiarinandrasana and R.Piques, *Damage and fracture of polyvinylidene fluoride (PVDF) at 20 °C: Experiments and modelling*, Engineering Fracture Mechanics, (2006).

[6] R. Schirrer and C.Fond and A.Lobbrecht, *Volume change and light scattering during mechanical damage in polymethylmethacrylate toughened with core-shell rubber particles*, Journal of Material Science, (1996).

[7] C. Regrain and L. Laiarinandrasana and S. Toillon and K. Saï, *Multi-mechanism models for semi-crystalline polymer: Constitutive relations and finite element implementation*, International Journal of Plasticity, (2008).
[8] K. Saï and L. Laiarinandrasana and I. Ben Naceur and J. Besson and M. Jeridi and G. Cailletaud, *Multi-mechanism damage-plasticity model for semi-crystalline polymer: Creep damage of notched specimen of PA6*, Materials Science and Engineering A, (2010).
[9] J.Besson and R.Foerch, *Large scale object-oriented finite element code design*, Comput. Methods Appl. Mech. Eng., (1997).
[10] J. Besson, *Damage of ductile materials deforming under multiple plastic or viscoplastic mechanisms*, International Journal of Plasticity, (2009).
[11] J. Besson and C. Guillemer-Neel, *An extension of the Green and Gurson models to kinematic hardening*, Mechanics of Materials, (2002).